Science Foundation.

[1]R. E. Aamodt and D. L. Book, Phys. Fluids 9, 143 (1966).
[2]H. L. Berk, M. N. Rosenbluth, and R. N. Sudan, Phys. Fluids 9, 1606 (1966).
[3]D. E. Baldwin, Phys. Rev. Lett. 18, 1119 (1967).
[4]H. L. Berk, C. W. Horton, M. N. Rosenbluth, and R. N. Sudan, Phys. Fluids 10, 2003 (1967).
[5]H. L. Berk, C. W. Horton, M. N. Rosenbluth, D. E. Baldwin, and R. N. Sudan, Phys. Fluids 11, 365 (1968).
[6]H. L. Berk, L. D. Pearlstein, and J. G. Cordey, Phys. Fluids 15, 891 (1972).
[7]C. W. Roberson, Ph.D. thesis, University of Texas, Austin, 1971 (unpublished).
[8]C. W. Roberson and K. W. Gentle, Phys. Fluids 14, 2462 (1971).

Laser Target Model*

N. K. Winsor
Naval Research Laboratory, Washington, D.C. 20375

and

D. A. Tidman
Science Applications Inc., Arlington, Virginia

(Received 10 August 1973)

Results of a numerical simulation model are presented. Internally generated megagauss magnetic fields are produced which tend to impede and deform the heat flow into the target plasma beyond the laser-energy deposition layer. Two new instabilities are also discussed.

A two-dimensional code has been developed for the processes involved in the interaction of a focused laser pulse with a moderate-atomic-weight target. A system of fluid equations including self-generated magnetic fields[1-3] is solved in cylindrical geometry by a second-order algorithm using time-step-split flux-corrected transport.[4] Interest in these plasmas derives from their potential application as pulsed x-ray sources,[5] ion sources, and possibly fusion. We shall present representative results of numerical simulations, demonstrate the importance of the self-generated magnetic field, and draw attention to two instabilities which may play a role in the physics of the laser-target interaction.

Typically, we consider nanosecond (or subnanosecond) Nd pulses with intensities $>10^{14}$ W/cm^2 through the focal spot, which give rise to target plasma temperatures above 1 keV. Thermal energy spreads from the laser focal region via electron thermal conduction, fluid expansion, and line and continuum emission from highly charged ion states. Magnetic fields in the megagauss range are generated internally in the plasma and tend to inhibit thermal conduction in the direction perpendicular to $\vec{B}$ in regions where $\Omega_e\tau_e>1$. Radiation pressure also plays a role for intensities $>10^{14}$ W/cm^2, but is not included in the present code.

The fluid equations used are

$$\partial N/\partial t+\nabla\cdot(N\vec{V})=0, \tag{1}$$

$$NM\,d\vec{V}/dt+\nabla\cdot[P\overleftrightarrow{I}+\overleftrightarrow{I}B^2/8\pi-\vec{B}\vec{B}/4\pi]=0, \tag{2}$$

$$\partial\mathcal{E}/\partial t+\nabla\cdot(\mathcal{E}\vec{V})=-P\nabla\cdot\vec{V}+\vec{J}\cdot\vec{E}'+\langle\delta\vec{E}\cdot\delta\vec{J}\rangle+R_e+\nabla\cdot(\overleftrightarrow{K}_e\cdot\nabla T_e), \tag{3}$$

$$P=C_P(\mathcal{E},N),\quad T_e=C_T(\mathcal{E},N), \tag{4}$$

$$\frac{\partial\vec{B}}{\partial t}=\nabla\times\left[\vec{V}\times\vec{B}-\frac{c^2}{4\pi}\overleftrightarrow{r}\cdot(\nabla\times\vec{B})\right]-\frac{ck}{eN_e}\nabla N_e\times\nabla T_e, \tag{5}$$

where

$$\vec{E}'=\vec{E}+\vec{V}\times\vec{B}/c=-(eN_e)^{-1}\nabla(ZNkT_e)+\overleftrightarrow{r}\cdot\vec{J}. \tag{6}$$

In these equations N is the total ion number density, $\langle\delta\vec{E}\cdot\delta\vec{J}\rangle$ the laser-energy deposition term, $P=NkT(1+Z)$ the total pressure, $\mathcal{E}$ the thermal plus ionization energy density, and R_e the rate of change of $\mathcal{E}$ due to radiation processes. The resistivity $\overleftrightarrow{r}$, and electron thermal conductivity $\overleftrightarrow{K}_e$, are taken from the work of Braginskii[1] with the $\vec{B}$ dependence of $\overleftrightarrow{r}$ and $\overleftrightarrow{K}_e$ included. The coronal model[6] calculates the distribution of ion charge states assuming equilibrium between electron collisional ionization and radiative recombination. It provides P and T_e as functions C_P and

C_T of $\mathcal{E}$ and N.

Laser-energy deposition by inverse bremsstrahlung is treated by an analytic path-integrated method which is energy conservative. Energy which reaches the critical density without being absorbed is deposited there. Emitted radiation is treated by a corona model but radiation transport is neglected. The thermal conductivity is not flux limited. The cases presented here (full dynamics and $B = 0$) have been run with and without flux limiting, and the results are nearly identical. Numerical experiments have been performed with Mg and higher-Z targets. Here we report the results of work with aluminum, which is representative.

We shall examine the effect of a laser pulse which is Gaussian in space and time (50-μm half-width, 1-nsec pulse length) which deposits 20 J in the target. The target is initially given by a solid region, plus an exponential density tail facing the laser, with a (small) uniform energy density, to approximate the state after a prepulse. The results we present here are insensitive to the initial tail parameters.

Figure 1 presents some important parameters versus distance along the incident laser beam. Two persistent features are the crossed density and temperature ramps [$\nabla N_e \times \nabla T_e$ is a source for $\vec{B}$ in Eq. (5)], and the separation of the critical-density region, where the absorption peaks, from the region of maximum radiation emission. This separation explains why a plasma which may be quite hot (several keV) at the critical density emits radiation characteristic of a much lower temperature. This is because of the N^2 dependence of the emission which causes the cooler overdense plasma to emit most rapidly. A total conversion efficiency from laser energy to radiation emission of ~ 6% was obtained for the case in Fig. 1. Higher radiation efficiencies are expected for higher-energy pulses.

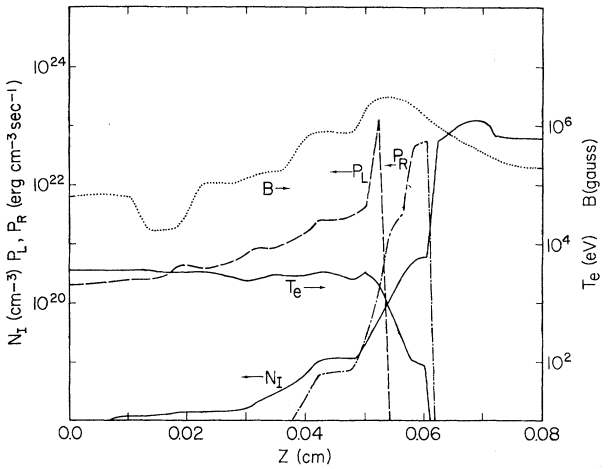

FIG. 1. Ion number density, temperature, magnetic field strength, laser absorption power, and radiated power, all versus distance into the target. Profiles are plotted for a radial distance of 40 μm from the axis of the incident beam at 1 nsec. The Nd laser pulse is assumed Gaussian, 50 μm radial half-width, 20 J total energy on target.

The ripples in the laser absorption profile correspond to an acoustic wave propagating toward the laser (left), and indicate the presence of an absorption instability characterized by a critical wavelength ($\lambda > \lambda_c$ unstable)

$$\lambda_c \cong 2\pi(K_\perp kT/3P_L)^{1/2}, \tag{7}$$

where P_L is the laser-deposition power density and $K_\perp$ the thermal conductivity perpendicular to $\vec{B}$. It results from the density dependence of the inverse bremsstrahlung absorption, coupling energy into acoustic modes. It is approximately density independent. Further, it is observed when $\vec{B}$ is present, i.e., $K_\perp$ small since $\Omega_e \tau_e \gg 1$, and tends not to be observed if $\vec{B} = 0$.

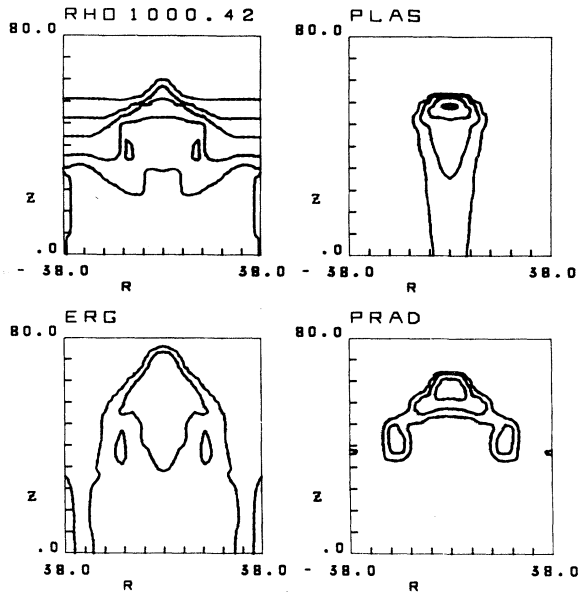

FIG. 2. Contours of ion mass density, laser absorption, energy density, and radiated power in the r-z plane for the case of Fig. 1. The laser is at the bottom, and the contoured region is 800×800 μm^2. In each box, the contour levels are order of magnitude, i.e., each contour represents 10 times more (or less) than the one next to it. The lowest levels are 10^{-5} g/cm^3 for the mass, 10^{11} erg/cm^3 for the energy, and 10^{20} erg/cm^3/sec for the laser and radiated power.

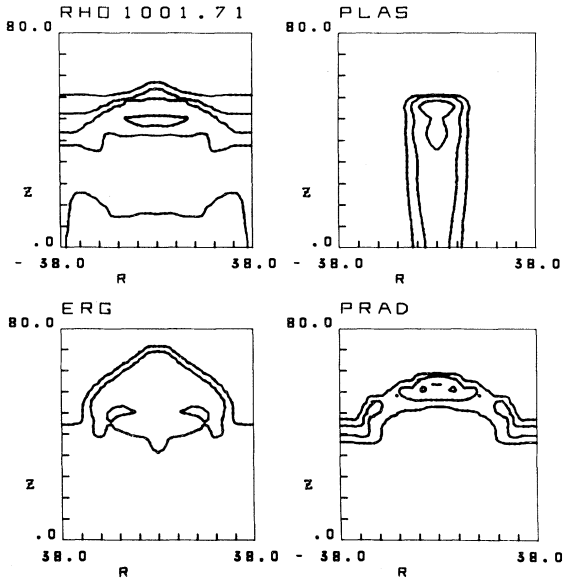

FIG. 3. Same plasma and contour parameters as Fig. 2, for the case $B=0$. Note the less rapid penetration of energy and density contours into the solid (top) and the lower radiation intensity. The radiation contours reaching the edges may be a result of numerical diffusion.

The magnetic field is a maximum in the region surrounding the peak absorption and radiation layers. This reduces heat transport there and allows large temperature gradients to develop. In addition it alters the convection of plasma. It would also play a role in suprathermal particle generation and transport.[7]

Figure 2 displays three of the parameters from Fig. 1, as contours in the r-z plane. Figure 3 provides the same information for a model consisting of Eqs. (1)–(4) with $\vec{B}=0$. Note the differences in the contours in Fig. 2, particularly near the axis.

In the numerical experiments displayed here, the field B is generated from nonuniformities in the laser intensity. However, one could ask whether field would be produced in uniformly irradiated targets, e.g., for a plane laser wave incident parallel to ∇N_e so the source term $\nabla N_e \times \nabla T$ vanishes in (5). In this case it turns out that a perturbation in the initially uniform temperature along the critical layer gives rise to a field $\vec{B}$ through the source $\nabla N_e \times \nabla T$, which in turn enhances the temperature perturbation, through $\vec{\vec{K}}_e(B)$. The most unstable wavelength for this thermal instability[8] is (for high-Z plasmas)

$$\lambda_M \cong 0.44\left[\frac{c\ln\Lambda}{(kT/m)^{1/2}}\frac{1}{N\lambda_D{}^3}\right]^{1/2}\left[\frac{\partial \ln N}{\partial x}\frac{\partial \ln T}{\partial x}\right]^{-1/2}.$$

For example, for $T=10^7$, $N=5\times10^{19}$, $Z=13$, $\partial \ln N/\partial x = \partial \ln T/\partial x = 10^2$ cm^{-1}, we find $\lambda_M \sim 3\times10^{-3}$ cm and a growth rate $\gamma \cong 2\times10^{11}$ sec^{-1}. The wavelength $\lambda_M \propto T^{3/4}$ and growth rate $\gamma \propto T^{5/2}$. Thus at higher temperatures, such as the 5×10^7 °K value in the computer experiments, λ_M becomes smaller than the grid size and is not present in Figs. 1–3.

It is a pleasure to acknowledge the assistance of D. Mosher with the corona model, and J. Gardner with the use of flux-corrected transport. The authors have enjoyed useful discussions with J. Davis and K. Whitney. More complete numerical surveys and analysis of the above instabilities will be published later.

*Work funded under Defense Nuclear Agency Subtask Grant No. W99QAXPF001-19.

[1]S. I. Braginskii, in *Reviews of Plasma Physics*, edited by M. A. Leontovich (Consultants Bureau, New York, 1965), p. 205.

[2]J. A. Stamper, K. Papadopoulos, S. O. Dean, E. A. McLean, and J. M. Dawson, Phys. Rev. Lett. 26, 1012 (1972).

[3]J. B. Chase, J. L. LeBlanc, and J. R. Wilson, Phys. Fluids 16, 1142 (1973).

[4]J. P. Boris and D. L. Book, J. Comput. Phys. 11, 38 (1973).

[5]See, e.g., Bull. Amer. Phys. Soc. 18, 684 (1973), abstracts HN5–HN14.

[6]D. Mosher, U. S. Naval Research Laboratory Report No. 2563, 1973 (unpublished).

[7]D. A. Tidman and J. A. Stamper, Appl. Phys. Lett. 22, 498 (1973).

[8]D. A. Tidman and R. A. Shanny, to be published.